

# Chemical/Molecular Structure of the Dentin–Enamel Junction is Dependent on the Intratooth Location

Changqi Xu · Xiaomei Yao · Mary P. Walker ·  
Yong Wang

Received: 15 July 2008 / Accepted: 2 December 2008 / Published online: 18 January 2009  
© Springer Science+Business Media, LLC 2009

**Abstract** The dentin–enamel junction (DEJ) plays an important role in preventing crack propagation from enamel into dentin. This function stems from its complex structure and materials properties that are different from either dentin or enamel. The molecular structural differences in both mineral and organic matrix across the DEJ zone were investigated by two-dimensional confocal Raman microspectroscopic mapping/imaging technique. The intensity ratios of 1450 (CH, matrix)/960 (P-O, mineral) decreased gradually to nearly zero across the DEJ. The width of this transition zone was dependent on the intratooth location, with  $12.9 \pm 3.2$   $\mu\text{m}$  width at occlusal positions and  $6.2 \pm 1.3$   $\mu\text{m}$  at cervical positions. The difference in width was significant ( $P < 0.001$ ). Concurrently, spectral differences in both organic and inorganic matrices across the DEJ were also noted. For example, the ratios of 1243 (amide III)/1450 (CH) within the DEJ were lower than the values in dentin; however, the ratios of 1665 (amide I)/1450 (CH) within the DEJ were higher than those values in dentin. In addition, the ratios of 1070 (carbonate)/960 (phosphate) within the dentin were lower than the values in the DEJ. Raman images indicated that the distribution of the above ratios across the DEJ zone were also different at occlusal and cervical positions. The results suggest that the intratooth-location-dependent structure of the DEJ may be related to its function. Micro-Raman spectroscopic/imaging analysis of the DEJ provides a powerful means of identifying the functional width and molecular structural differences across the DEJ.

**Keywords** Dentin–enamel junction (DEJ) · Molecular structure · Confocal Raman microspectroscopic mapping/imaging

The human tooth—or more specifically, the tooth's crown—is composed of dentin covered by enamel. Dentin, which is derived from the mesoderm, is a flexible, mineralized tissue composed of 70% (weight%) inorganic material, 20% organic material, and 10% fluid. In contrast, enamel, which is derived from ectoderm, is a very brittle tissue composed of mostly hydroxyapatite mineral ( $\sim 96\%$ ), water ( $\sim 3\%$ ), and trace organic matrix ( $\sim 1\%$ ) [1]. Thus, the dentin–enamel junction (DEJ) is an interface between two mineralized tissues with different compositions and biomechanical properties [2]. The DEJ is believed to play an important role in preventing crack propagation from enamel to dentin and inhibiting further catastrophic tooth fracture.

The complex microstructure and composition of the DEJ at various levels is supposedly linked to its function as an effective obstacle for crack propagation. The DEJ structure has been described as a series of 25–200- $\mu\text{m}$ -diameter scallops that contain 80–120-nm parallel type I collagen fibrils extending from the dentin into enamel, which might play a role in crack prevention [3]. Crack deflection near the DEJ has also been potentially linked to a mechanical property gradient, i.e., modulus, across the zone [4–9]. The modulus gradient has been associated with variations of mineralization and the associated collagen-to-mineral ratio within the DEJ compared with dentin and enamel [5, 7, 10]. Recently, finite-element models [11] showed that in the scallop model, the net compression toward the DEJ was consistently higher than net tension away from it. As a consequence, the dentin and enamel would be pushed toward each other during loading.

C. Xu · X. Yao · M. P. Walker · Y. Wang (✉)  
Department of Oral Biology, University of Missouri-Kansas City  
School of Dentistry, 650 E. 25th St., Kansas City, MO 64108,  
USA  
e-mail: Wangyo@umkc.edu

Because of this crack-prevention function, the physical properties—for example, the width, microhardness, and elastic modulus of the DEJ—become critical information. So far, the conclusions on these issues have been in disagreement. Nanoindentation was carried out by using a range of 40 to 60  $\mu\text{m}$  across the DEJ zone with loads up to 30,000  $\mu\text{N}$ . The values of modulus and hardness decreased from  $E = 65$  GPa and  $H = 3.5$  GPa in the enamel region to  $E = 20$  GPa and  $H = 0.7$  GPa in the dentin region. An average DEJ width range of 11.8  $\mu\text{m}$  was identified [6]. The results from microindentation measurements [1] revealed similar hardness and modulus values. However, another study [12] showed that the microhardness gradient occurred within  $\sim 100$ - $\mu\text{m}$  range. Some results from optical spectroscopy [13] showed that the median DEJ width was 10  $\mu\text{m}$ , ranging from 7 to 15  $\mu\text{m}$ , which was similar to the width obtained from the nanoindentation method. However, previous results did not seem to be dependent on the intratooth location [6, 13].

Although the previous studies provide useful information for understanding the DEJ morphology and the associated mechanical properties, to date, there has been no in-depth analysis of the DEJ's chemical structure at the molecular level. The chemical structural information is critical for a more complete understanding of crack-prevention behavior in the DEJ zone because material properties are dependent on the material chemical composition. This information is also critical in terms of being able to create a biomimetic approach for connecting dissimilar biomaterials.

Confocal micro-Raman spectroscopy has been widely used to investigate the chemical/molecular structure of various materials and tissues [14–18] because of its many advantages, including minimal specimen preparation and noninvasive sampling capability. In addition, compound-specific molecules can be detected with little spectral interference from  $\text{H}_2\text{O}$ . As a result, it has been introduced into the biophysics field to obtain the molecular structure information for both in vivo [19, 20] and in vitro studies [15, 21, 22]. Raman microscopy's high spectral resolution (up to  $1\text{ cm}^{-1}$ ) and high spatial resolution (up to 1  $\mu\text{m}$ ) make it an excellent tool for mapping the components of the DEJ specimens at the micrometer level. Therefore, the purpose of this investigation was to characterize the molecular/structural differences across the DEJ zone with two-dimensional confocal Raman microspectroscopic mapping/imaging technique.

## Materials and Methods

### Specimen Preparation

Five noncarious, human third molars were collected according to the protocol approved by the University of

Missouri-Kansas City adult health sciences institutional review board. After removing any remaining soft tissues, the extracted teeth were stored at  $4^\circ\text{C}$  in 0.9% phosphate-buffered saline (PBS) with 0.002% sodium azide added to inhibit bacterial and fungal contamination (pH 7.4). A slow-speed water-cooled diamond saw (Buehler Ltd., Lake Bluff, IL), was used to remove the roots from the molars. The remaining crowns were then sectioned buccolingually to generate a 2-mm-thick cross-sectional slice centered on the mesiobuccal and mesiolingual cusps. The specimens with the exposed DEJ were further manually polished under water with 600-grit SiC paper. To prevent dehydration, all sectioned specimens were placed into PBS solution, and Raman microscopic analysis immediately followed.

### Raman Microspectroscopy and Imaging

A LabRam HR 800 Raman spectrometer (Horiba Jobin Yvon, Edison, NJ) using monochromatic radiation emitted by a He-Ne laser (632.8 nm) and operating at excitation power of 20 mW was used to collect Raman spectra and images. It was equipped with a confocal microscope (Olympus BX41), a piezoelectric (PI) XYZ stage with a minimum step width of 50 nm, and an air-cooled CCD detector of  $1024 \times 256$  pixels. During Raman imaging, the following parameters were used: 600 grating, 140- $\mu\text{m}$  confocal hole, and 100- $\mu\text{m}$  slit width. Spectra were Raman-shift-frequency calibrated with known lines of silicon.

Specimens were removed from the PBS and placed into distilled water for the micro-Raman analysis. Micro-Raman spectra with a  $\times 100$  water immersion objective (Olympus, 1.00w) focused on the specimens. With the optical DEJ used as a landmark, mapping spectra were acquired at positions corresponding to 1- $\mu\text{m}$  intervals across a 35- $\mu\text{m}$  length via computer-controlled x-y-z stage. Spectra were obtained over the spectral region of 400 to  $1750\text{ cm}^{-1}$  and with a 90-s integration time. Six spectral maps were obtained at the buccal cusp and cervical area of each specimen (Fig. 1). An imaging system and high-resolution monitor enabled visual identification of the position at which the Raman spectra were obtained.

### Spectral Data Analysis

Labspec 5 software (Horiba Jobin Yvon) was used to analyze the acquired Raman spectra and mapping data. Without additional spectral smoothing, the individual spectra were adjusted by multiple-point baseline correction, and mapping spectra for imaging were adjusted by polynomial baseline correction. Two representative Raman spectra obtained from dentin and enamel are shown in Fig. 2. The peaks at  $960\text{ cm}^{-1}$  are assigned to  $\nu_1$  vibration

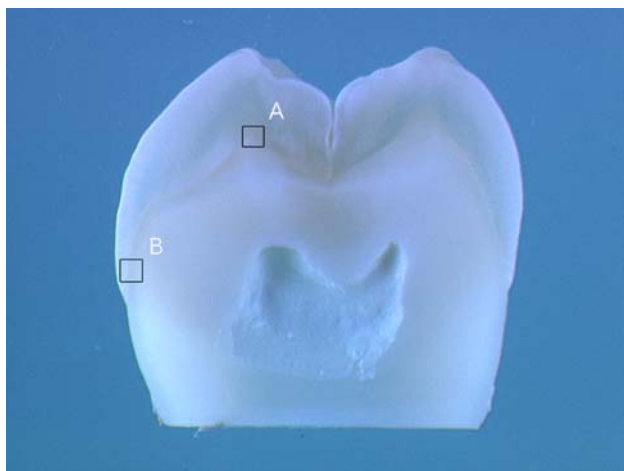


**Fig. 1** Representative photograph of a cross-sectional tooth slice illustrating where spectral maps were obtained at the buccal cusp and cervical area. (A) Buccal mapping area. (B) Cervical mapping area

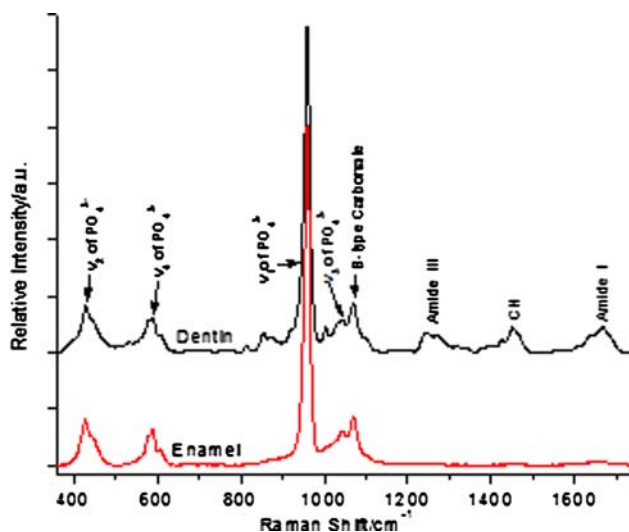


**Fig. 2** Representative Raman spectra of dentin and enamel

peak of phosphate group in mineral. The peak at  $1070\text{ cm}^{-1}$  is assigned to  $\nu_1$  vibration of carbonate group (B type of carbonate) from mineral. In addition, the peaks at  $1246/1270\text{ cm}^{-1}$ ,  $1450\text{ cm}^{-1}$ , and  $1667\text{ cm}^{-1}$  are assigned to amide III, CH, and amide I from organic components. The  $\nu_1$  vibration peak of phosphate at  $960\text{ cm}^{-1}$  was selected as the internal standard for the normalization adjustment (Fig. 2).

Raman images based on the ratios of CH at  $1450\text{ cm}^{-1}$  to  $\nu_1$  of phosphate at  $960\text{ cm}^{-1}$  were obtained to measure organic matrix mineral content. By means of the generated mapping spectra, the width of the DEJ was measured on the basis of the matrix mineral ratios at occlusal and cervical sites. The mean DEJ width of each site/tooth was calculated on the basis of the six maps per site. A one-way analysis of variance ( $\alpha = 0.05$ ) was used to analyze the

DEJ width as a function of tooth location (occlusal versus cervical).

In addition, after normalization adjustment based on the CH stretching peak at  $1450\text{ cm}^{-1}$ , Raman images based on the ratios of amide I at  $1667\text{ cm}^{-1}$  to CH peak at  $1450\text{ cm}^{-1}$  and the ratios of amide III at  $1240\text{--}1270\text{ cm}^{-1}$  to CH peak at  $1450\text{ cm}^{-1}$  were obtained. The ratios of B-type carbonate at  $1070\text{ cm}^{-1}$  to  $\nu_1$  of phosphate at  $960\text{ cm}^{-1}$  were obtained to analyze differences in mineral composition across the specimens.

## Results

Representative Raman mapping results of the DEJ at occlusal and cervical sites of a human molar are shown in Fig. 3a, b, respectively. Raman images were obtained on the basis of the intensity ratios of CH at  $1450\text{ cm}^{-1}$  (matrix) to phosphate at  $960\text{ cm}^{-1}$  (mineral). The relative matrix/mineral ( $1450/960$ ) ratios are represented by the color differences. Yellow/white represents higher relative

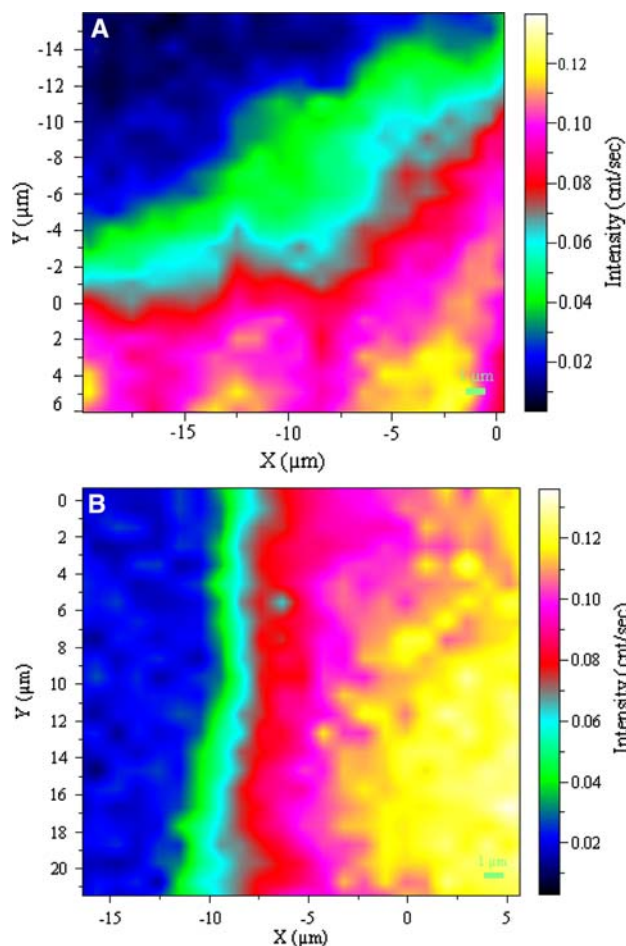


**Fig. 3** Representative Raman image of the DEJ based on intensity ratios of  $1450/960$  at **a** occlusal and **b** cervical positions

intensity ratios, while black/dark blue represents lower ratios. A region where the color gradually changes from blue to red or pink is related to the DEJ transition zone. Comparison of the two images indicated that the width of the transition zone at the occlusal position was wider than that at the cervical position. The representative relationships of the matrix/mineral (1450/960) ratios as a function of positions across the DEJ transition zone are shown in Fig. 4a, b. The matrix/mineral ratios of the DEJ were higher than those of enamel and lower than those of dentin. These ratios of the DEJ gradually increased during the transition from the enamel to dentin zone. The widths of the transition zone were measured across five teeth (Table 1). There was a significant difference ( $P < 0.001$ ) between the overall mean occlusal DEJ width,  $12.9 \pm 3.2 \mu\text{m}$ , and the cervical DEJ width,  $6.3 \pm 1.3 \mu\text{m}$ .

Raman spectra from the dentin and DEJ zone in the protein-derived spectral region of  $1200\text{--}1750 \text{ cm}^{-1}$  are shown in Fig. 5a, b, in which the vibration peak of CH at  $1450 \text{ cm}^{-1}$

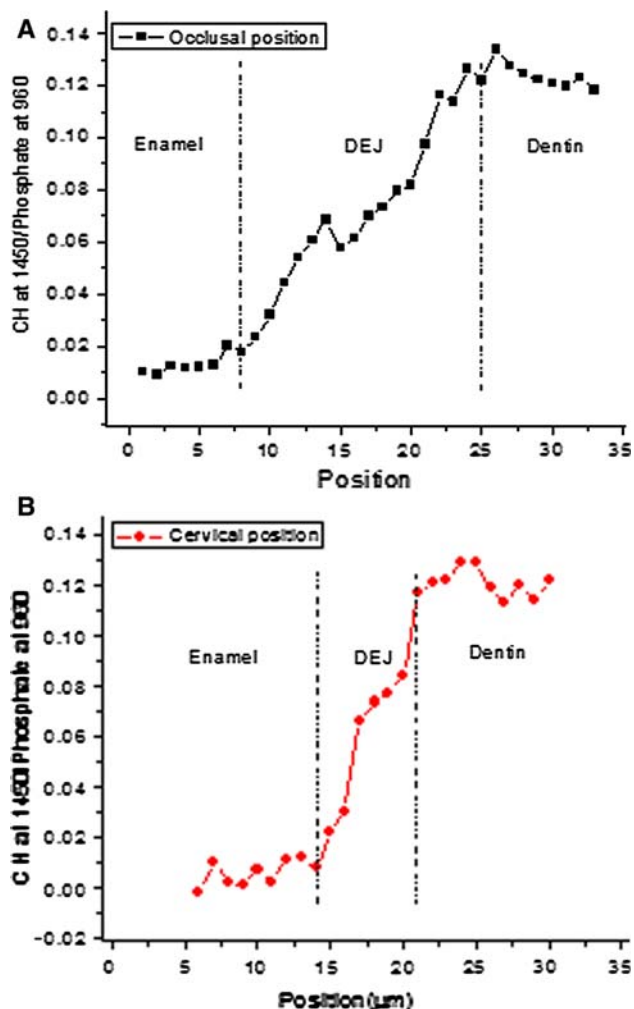


**Fig. 4** Relative intensity ratios of 1450/960 across the enamel/DEJ/dentin zone at **a** occlusal and **b** cervical positions

**Table 1** Occlusal and cervical dentin–enamel junction (DEJ) transition zone mean width and standard deviation ( $\mu\text{m}$ )

Tooth	Buccal cusp occlusal site	Buccal cervical site
1	$10.8 \pm 3.5$	$6.3 \pm 1.4$
2	$12.2 \pm 2.6$	$6.0 \pm 0.9$
3	$12.7 \pm 2.8$	$5.8 \pm 1.0$
4	$14.2 \pm 2.5$	$6.2 \pm 1.5$
5	$14.8 \pm 3.3$	$7.3 \pm 1.8$
Overall*	$12.9 \pm 3.2$	$6.3 \pm 1.3$

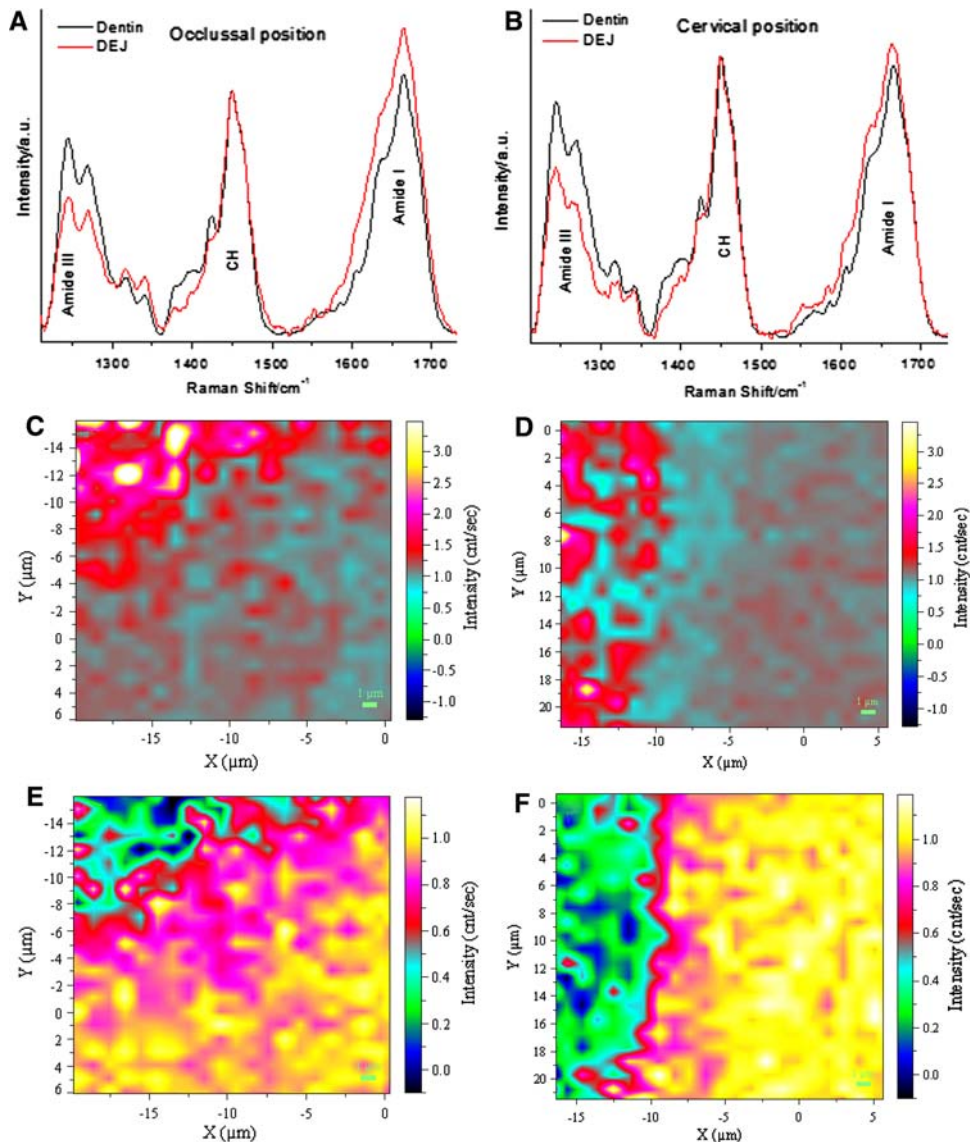
$N = 30$  Raman mappings/site (six measurements per site per tooth)

\* There was a significant difference ( $P < 0.001$ ) in DEJ width between sites

was selected as internal standard for the normalization adjustment. As compared with dentin spectra, the amide I peak increased, but the amide III peak decreased in the DEJ spectra. In addition, evaluation of the spectra also shows notable changes in protein-derived peaks in the regions of  $1350\text{--}1430 \text{ cm}^{-1}$  and  $1550\text{--}1600 \text{ cm}^{-1}$ . For example, there was a pronounced peak at approximately  $1425 \text{ cm}^{-1}$  in the dentin spectra, but this peak was not obvious in the DEJ spectra. The relative intensities of the peaks at approximately  $1380$  and  $1396 \text{ cm}^{-1}$  were higher in the dentin spectra. The above results indicated that molecular structure of organic matrix in the DEJ was different from that in dentin. The distinctions in organic matrix and its distribution across the DEJ zone at occlusal positions and cervical positions were observed when Raman images were obtained on the basis of the relative intensity ratios of the peaks from amide I–III spectral regions (Fig. 5c–f). In the amide I/CH images, the values from the intensity ratios of 1667 to 1450 were non-uniformly distributed in the zone across the enamel to dentin. Overall, these values were higher in the enamel zone than those in the dentin zone. However, the DEJ zones at both occlusal and cervical positions were not distinguishable within those images. In contrast to the amide I/CH images, in the amide III/CH images, the values from the intensity ratios were lower in the enamel zone and higher in the dentin zone. The DEJ zone was distinguishable in the amide III/CH images, with the DEJ being wider at the occlusal position (Fig. 5). The above results indicate that the molecular structure of organic matrix varied between dentin, enamel, and DEJ, and was also dependent on the intratooth location.

Raman spectra from the dentin and DEJ zone in the spectral region of  $900\text{--}1150 \text{ cm}^{-1}$  are shown in Fig. 6a, b. The spectra were normalized on the basis of the  $960 \text{ cm}^{-1}$  phosphate peak. Evaluation of the spectra shows some notable changes in mineral-derived peaks. For example, compared with dentin spectra, the relative intensities of the carbonate peak at  $1070 \text{ cm}^{-1}$  (B type of carbonate) increased in the DEJ spectra at both occlusal and cervical

**Fig. 5** Raman spectra in protein-derived spectral regions from dentin and the DEJ at occlusal positions (a) and at cervical positions (b); representative Raman image of the DEJ based on intensity ratios of amide I/1450 at occlusal positions (c) and at cervical positions (d); representative Raman image of the DEJ based on intensity ratios of amide III/1450 at occlusal positions (e) and at cervical positions (f)



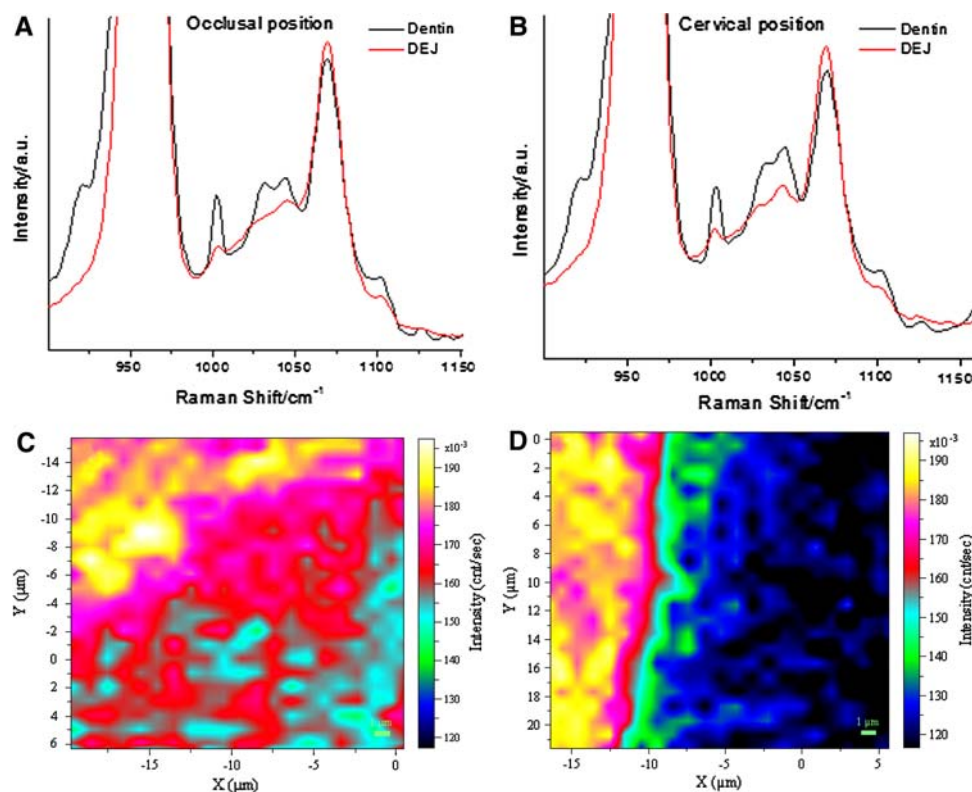
positions. The distribution of 1070/960 ratios across the DEJ zone at occlusal positions and cervical positions is shown in Fig. 6c, d. Overall, the values of these ratios indicated that the content of type B carbonate in enamel was relatively higher than that in dentin. At the cervical position, the type B carbonate content gradually decreased from the enamel to dentin, and the DEJ zone was uniform. However, at the occlusal position, the DEJ zone was not distinguishable in the image (Fig. 6c), indicating the distribution of the type B carbonate content was more heterogeneous and complicated across the occlusal DEJ zone.

## Discussion

The DEJ as an interface between two materials with dissimilar composition and properties has been identified since

1835 [23]. However, there have been inconsistent conclusions reported about the functional width of the DEJ zone as a result of measurements with different instruments with diverse spatial resolutions. For example, when traditional fracture mechanics [4] in combination with the scanning electron microscopy (SEM) approach was used, the width of the DEJ zone was reported as a functional width of 50 to 100  $\mu\text{m}$ , which was the deviation depth of the associated crack path. Furthermore, a Vickers microhardness profile [12] obtained with loads of 15 g across the DEJ revealed a broad transition zone of  $\sim 100 \mu\text{m}$ . However, with the nanoindentation method [6], although similar values of hardness and elastic modulus were reported as compared with previous studies, the DEJ width was much smaller ( $\sim 12 \mu\text{m}$ ). By means of a new modulus mapping technique, the same group of investigators reported a DEJ width as low as 2–3  $\mu\text{m}$  [24]. The variations in width measurements can be

**Fig. 6** Raman spectra in mineral-derived spectral regions from dentin and the DEJ at occlusal positions (a); at cervical positions (b); representative Raman image of the DEJ based on intensity ratios of 1070/960 at occlusal positions (c); at cervical positions (d)



explained not only by the differences in the spatial resolutions of the instruments, but also by whether the matrices surrounding the interface were included in the measurements. Goldberg et al. suggested that the DEJ is not a simple inert interface between two mineralized structures, but instead should be regarded as a complex that includes the inner aprismatic enamel and the mantle dentin [25].

In the present study, the chemical composition profiles (matrix/mineral ratios) were used to measure the width of the DEJ as a function of tooth position (Fig. 4). The intensity ratios of 1450 (CH, matrix)/960 (P-O, mineral) remained unchanged in dentin, then decreased gradually to nearly zero across the DEJ. The width of this transition zone was determined to be in the range of 5–16  $\mu\text{m}$ . Interestingly, on the basis of the matrix/mineral ratios, it was shown that the mean DEJ width was  $12.9 \pm 3.2 \mu\text{m}$  at occlusal positions and  $6.3 \pm 1.3 \mu\text{m}$  at cervical positions. Previous research has shown that the enamel initially forms at the occlusal/cuspal locations, followed by enamel formation across the crown to the cervical area [26, 27]. The difference in development times of enamel at occlusal and cervical positions might account for the difference in structural width of the DEJ between positions. The difference might also be related to differences in function, with the occlusal surfaces exposed to greater loads during mastication than the cervical area.

The difference in DEJ width dependent on intratooth location has not been previously reported in investigations

that used measurements of mechanical properties, such as hardness or modulus. The direct relationship between mechanical properties and chemical compositions across the DEJ zone needs to be further explored and correlated. However, it is expected that the mechanical properties might not be directly related to chemical compositions such as the matrix/mineral ratios. Many other factors, such as porous structure within the DEJ complex, may also affect the mechanical properties. But the chemical structural information obtained in this study is critical in understanding the function of this DEJ complex.

To date, there has been minimal chemical information related to the DEJ transition zone as a result of its small size. The current micro-Raman results indicate that both chemical structure and composition of organic and inorganic matrices within the DEJ zone are different from either dentin or enamel. In terms of organic matrix, the spectral region of amides I and III was thought to be the best possible region for studying the protein structural changes [28, 29]. The position and intensity of these amide bands are sensitive to the molecular conformation/structure of the polypeptide chains [30] and/or orientation of collagen/proteins [31]. To separate the orientation effects from molecular/structural changes, we collected spectra before and after rotating the specimens. The differences in the dentin and DEJ spectra were unchanged and were insensitive to orientation effects. This indicated that the spectral differences were mainly due to molecular/structural changes. In a comparison of the

amides region in the spectra of dentin and DEJ (Fig. 5), the amide I peak increased but the amide III peak decreased in the DEJ spectra. In the images of amide I/CH and amide III/CH, the distribution of these ratios was more heterogeneous in the DEJ transition zone. Besides the amides region, the differences in the region of 1350–1430  $\text{cm}^{-1}$  were also noticeable (Fig. 5). The peaks in this region were pronounced in the dentin spectra. The peaks at approximately 1380, 1396, and 1425  $\text{cm}^{-1}$  are associated with  $\text{CH}_2$  deformation [32, 33]. The peak at approximately 1396  $\text{cm}^{-1}$  is usually seen in native collagen [33]. The decrease in these peak intensities might be associated with increasing disorder of the functional groups in organic matrix [32]. These spectral changes indicate that the structure of organic matrix in the dentin and DEJ was diverse. Formation of the DEJ begins at the early stages of tooth morphogenesis and is thought to be linked to a mixture of dentin proteins secreted by odontoblasts and enamel proteins from ameloblasts [34–36]. The proteins associated with DEJ formation and collagen fibril bundles that cross the transition zone and insert into enamel [3] might be responsible for the variations and distribution deviations in composition and structure of the organic matrix within the DEJ.

In terms of inorganic matrix variations, it was revealed that the crystal structure of mineral in enamel and dentin is different [37–39]. On the basis of our micro-Raman results, the position, shape, and width of phosphate peak at 960  $\text{cm}^{-1}$  were similar to those for dentin (data not shown), indicating the mineral crystallinity within the DEJ is not much different from the mineral in dentin. However, the intensity ratios of peak at 1070 to 960  $\text{cm}^{-1}$  increased from dentin to enamel across the DEJ zone, indicating a higher carbonate content in enamel. However, further Raman study indicated that this relatively higher carbonate content was demonstrated in only a narrow enamel region adjacent to the DEJ (data not shown). For enamel close to the tooth surface, the carbonate content was reported to be minimal—much lower than that in dentin [40]. These differences in carbonate content are important because the higher the carbonate level, the more susceptible to mineral dissolution [10, 41, 42]. Thus, minimal carbonate at the outer enamel surface should provide better resistance to attack from the acidic by-products associated with dental plaque. However, the increased carbonate within enamel near the DEJ may help explain why dental decay tends to penetrate more rapidly once it nears the DEJ [43].

Besides the difference in width based on matrix/mineral intensity ratios, the intratooth-location-dependent structure of the DEJ was also noticed in other Raman intensity ratios. At cervical positions, the interfacial margins were easily visible in the images from different intensity ratios. For example, these margins usually appeared at  $x$  position of approximately  $-10 \mu\text{m}$ , and the interfacial zone was

relatively uniform across the DEJ. However, at occlusal positions, the margins were hard to differentiate and appeared at different positions in the images from different intensity ratios. The overall interfacial zone was not uniform and was more heterogeneous compared with that at cervical positions.

In summary, Raman spectroscopy equipped with confocal microscope proved to be useful in investigating the microstructure of the DEJ at the micrometer scale. The Raman results suggest there are difference in the DEJ width as function of intratooth location along with differences in the DEJ organic and inorganic components between the occlusal and cervical sites.

**Acknowledgments** This investigation was supported in part by USPHS research grants DE 015735, DE 015281, and DE 016023 from the National Institute of Dental and Craniofacial Research, National Institutes of Health, Bethesda, MD.

## References

- Xu HHK, Smith DT, Jahanmir S, Romberg E, Kelly JR, Thompson VP, Rekow ED (1998) Indentation damage and mechanical properties of human enamel and dentin. *J Dent Res* 77:472–480
- Walker MP, Fricke BA (2006) Dentin–enamel junction of human teeth. In: Akay M (ed) Wiley encyclopedia of biomedical engineering. Wiley, Hoboken, pp 1061–1064
- Lin CP, Douglas WH, Erlandsen SL (1993) Scanning electron microscopy of type I collagen at the dentin–enamel junction of human teeth. *J Histochem Cytochem* 41:381–388
- Lin CP, Douglas WH (1994) Structure–property relations and crack resistance at the bovine dentin–enamel junction. *J Dent Res* 73:1072–1078
- Dong XD, Ruse ND (2003) Fatigue crack propagation path across the dentinoenamel junction complex in human teeth. *J Biomed Mater Res A* 66A:103–109
- Marshall GW Jr, Balooch M, Gallagher RR, Gansky SA, Marshall SJ (2001) Mechanical properties of the dentinoenamel junction: AFM studies of nanohardness, elastic modulus, and fracture. *J Biomed Mater Res* 54:87–95
- Fong H, Sarikaya M, White SN, Snead ML (2000) Nano-mechanical properties profiles across dentin–enamel junction of human incisor teeth. *Mater Sci Eng C Biomimet Supramolec Syst* 7:119–128
- Urabe I, Nakajima S, Sano H, Tagami J (2000) Physical properties of the dentin–enamel junction region. *Am J Dent* 13:129–135
- Maev RG, Denisova LA, Maeva EY, Denisov AA (2002) New data on histology and physico-mechanical properties of human tooth tissue obtained with acoustic microscopy. *Ultrasound Med Biol* 28:131–136
- WentrupByrne E, Armstrong CA, Armstrong RS, Collins BM (1997) Fourier transform Raman microscopic mapping of the molecular components in a human tooth. *J Raman Spectrosc* 28:151–158
- Shimizu D, Macho GA (2007) Functional significance of the microstructural detail of the primate dentino–enamel junction: a possible example of exaptation. *J Hum Evol* 52:103–111
- White SN, Paine ML, Luo W, Sarikaya M, Fong H, Yu ZK, Li ZC, Snead ML (2000) The dentino–enamel junction is a broad

- transitional zone uniting dissimilar bioceramic composites. *J Am Ceram Soc* 83:238–240
13. Gallagher RR, Demos SG, Balooch M, Marshall GW Jr, Marshall SJ (2003) Optical spectroscopy and imaging of the dentin–enamel junction in human third molars. *J Biomed Mater Res A* 64: 372–377
  14. Baena JR, Lendl B (2004) Raman spectroscopy in chemical bioanalysis. *Curr Opin Chem Biol* 8:534–539
  15. Darvin ME, Gersonde I, Ey S, Brandt NN, Albrecht H, Gonchukov SA, Sterry W, Lademann J (2004) Noninvasive detection of beta-carotene and lycopene in human skin using Raman spectroscopy. *Laser Phys* 14:231–233
  16. Katz A, Kruger EF, Minko G, Liu CH, Rosen RB, Alfano RR (2003) Detection of glutamate in the eye by Raman spectroscopy. *J Biomed Opt* 8:167–172
  17. Pappas D, Smith BW, Winefordner JD (2000) Raman spectroscopy in bioanalysis. *Talanta* 51:131–144
  18. Sayari A, Hamoudi S (2001) Periodic mesoporous silica-based organic–inorganic nanocomposite materials. *Chem Mater* 13: 3151–3168
  19. Schut TCB, Wolthuis R, Caspers PJ, Puppels GJ (2002) Real-time tissue characterization on the basis of in vivo Raman spectra. *J Raman Spectrosc* 33:580–585
  20. Shim MG, Wilson BC, Marple E, Wach M (1999) Study of fiber-optic probes for in vivo medical Raman spectroscopy. *Appl Spectrosc* 53:619–627
  21. Tsuda H, Arends J (1997) Raman spectroscopy in dental research: a short review of recent studies. *Adv Dent Res* 11:539–547
  22. Stone N, Kendall C, Smith J, Crow P, Barr H (2004) Raman spectroscopy for identification of epithelial cancers. *Faraday Discuss* 126:141–157
  23. Fraenkel L (1835) *De penitiori dentium humanorum structura observationis*. In: *Diss Vratislaviae*. Pressburg, Hungary
  24. Balooch G, Marshall GW, Marshall SJ, Warren OL, Asif SA, Balooch M (2004) Evaluation of a new modulus mapping technique to investigate microstructural features of human teeth. *J Biomech* 37:1223–1232
  25. Goldberg M, Septier D, Bourd K, Hall R, Jeanny JC, Jonet L, Colin S, Tager F, Chaussain-Miller C, Garabedian M, George A, Goldberg H, Menashi S (2002) The dentino–enamel junction revisited. *Connect Tissue Res* 43:482–489
  26. Reid DJ, Dean MC (2006) Variation in modern human enamel formation times. *J Hum Evol* 50:329–346
  27. Smith TM, Toussain M, Reid DJ, Olejniczak AJ, Hublin JJ (2007) Rapid dental development in a Middle Paleolithic Belgian Neanderthal. *Proc Natl Acad Sci USA* 104:20220–20225
  28. Frushour BG, Koenig JL (1975) Raman scattering of collagen, gelatin, and elastin. *Biopolymers* 14:379–391
  29. Wang Y, Spencer P (2002) Analysis of acid-treated dentin smear debris and smear layers using confocal Raman microspectroscopy. *J Biomed Mater Res* 60:300–308
  30. Renugopalakrishnan V, Carreira LA, Collette TW, Dobbs JC, Chandraksasan G, Lord RC (1998) Non-uniform triple helical structure in chick skin type I collagen on thermal denaturation: Raman spectroscopic study. *Z Naturforsch [C]* 53:383–388
  31. Kazanci M, Roschger P, Paschalis EP, Klaushofer K, Fratzl P (2006) Bone osteonal tissues by Raman spectral mapping: orientation–composition. *J Struct Biol* 156:489–496
  32. Kubisz L, Polomska M (2007) FT NIR Raman studies on gamma-irradiated bone. *Spectrochim Acta A Mol Biomol Spectrosc* 66:616–625
  33. Jastrzebska M, Wrzalik R, Kocot A, Zalewska-Rejdak J, Cwalina B (2003) Raman spectroscopic study of glutaraldehyde-stabilized collagen and pericardium tissue. *J Biomater Sci Polym Ed* 14:185–197
  34. Begue-Kim C, Krebsbach PH, Bartlett JD, Butler WT (1998) Dentin sialoprotein, dentin phosphoprotein, enamelysin and ameloblastin: tooth-specific molecules that are distinctively expressed during murine dental differentiation. *Eur J Oral Sci* 106:963–970
  35. Nagano T, Oida S, Ando H, Gomi K, Arai T, Fukae M (2003) Relative levels of mRNA encoding enamel proteins in enamel organ epithelia and odontoblasts. *J Dent Res* 82:982–986
  36. Nanci A, Zalzal S, Lavoie P, Kunikata M, Chen W, Krebsbach PH, Yamada Y, Hammarstrom L, Simmer JP, Fincham AG, Snead ML, Smith CE (1998) Comparative immunochemical analyses of the developmental expression and distribution of ameloblastin and amelogenin in rat incisors. *J Histochem Cytochem* 46:911–934
  37. Chiang YC, Lee BS, Wang YL, Cheng YA, Chen YL, Shiau JS, Wang DM, Lin CP (2008) Microstructural changes of enamel, dentin–enamel junction, and dentin induced by irradiating outer enamel surfaces with CO<sub>2</sub> laser. *Lasers Med Sci* 23:41–48
  38. Moreno EC, Aoba T (1991) Comparative solubility study of human dental enamel, dentin, and hydroxyapatite. *Calcif Tissue Int* 49:6–13
  39. Tramini P, Pelissier B, Valcarcel J, Bonnet B, Maury L (2000) A Raman spectroscopic investigation of dentin and enamel structures modified by lactic acid. *Caries Res* 34:233–240
  40. Robinson C, Shore RC, Brookes SJ, Strafford S, Wood SR, Kirkham J (2000) The chemistry of enamel caries. *Crit Rev Oral Biol Med* 11:481–495
  41. Gron P, Spinelli M, Trautz O, Brudevold F (1963) The effect of carbonate on the solubility of hydroxylapatite. *Arch Oral Biol* 8:251–263
  42. Legeros RZ, Trautz OR, Legeros JP, Klein E, Shirra WP (1967) Apatite crystallites: effects of carbonate on morphology. *Science* 155:1409–1411
  43. Roberson TM (2002) Cariology: the lesion, etiology, prevention, and control. In: Roberson TM, Heymann HO, Swift EJ (eds) *Sturdevant’s art and science of operative dentistry*. Mosby Elsevier, St Louis, pp 65–132